Original Article | Neuroimaging and Head & Neck

eISSN 2005-8330
https://doi.org/10.3348/kjr.2020.0949
Korean J Radiol 2021;22(5):759-769

Korean Journal of Radiology
KJR

Laplacian-Regularized Mean Apparent Propagator-MRI in Evaluating Corticospinal Tract Injury in Patients with Brain Glioma

Rifeng Jiang, PhD[1]*, Shaofan Jiang, MS[1]*, Shiwei Song, PhD[2], Xiaoqiang Wei, MS[2], Kaiji Deng, MS[1], Zhongshuai Zhang, PhD[3], Yunjing Xue, PhD[1]

Departments of [1]Radiology and [2]Neurosurgery, Fujian Medical University Union Hospital, Fuzhou, China; [3]MR Scientific Marketing, Siemens Healthcare, Shanghai, China

Objective: To evaluate the application of laplacian-regularized mean apparent propagator (MAPL)-MRI to brain glioma-induced corticospinal tract (CST) injury.

Materials and Methods: This study included 20 patients with glioma adjacent to the CST pathway who had undergone structural and diffusion MRI. The entire CSTs of the affected and healthy sides were reconstructed, and the peritumoral CSTs were manually segmented. The morphological characteristics of the CST (track number, average length, volume, displacement of the affected CST) were examined and the diffusion parameter values, including fractional anisotropy (FA), mean diffusivity (MD), axial diffusivity (AD), radial diffusivity (RD), mean squared displacement (MSD), q-space inverse variance (QIV), return-to-origin probability (RTOP), return-to-axis probabilities (RTAP), and return-to-plane probabilities (RTPP) along the entire and peritumoral CSTs, were calculated. The entire and peritumoral CST characteristics of the affected and healthy sides as well as those relative CST characteristics of the patients with motor weakness and normal motor function were compared.

Results: The track number, volume, MD, RD, MSD, QIV, RTAP, RTOP, and RTPP of the entire and peritumoral CSTs changed significantly for the affected side, whereas the AD and FA changed significantly only in the peritumoral CST ($p < 0.05$). In patients with motor weakness, the relative MSD of the entire CST, QIV of the entire and peritumoral CSTs, and the AD, MD, RD of the peritumoral CST were significantly higher, whereas the RTPP of the entire and peritumoral CSTs and the RTOP of the peritumoral CST were significantly lower than those in patients with normal motor function ($p < 0.05$ for all). In contrast, no significant changes were found in the CST morphological characteristics, FA, or RTAP ($p > 0.05$ for all).

Conclusion: MAPL-MRI is an effective approach for evaluating microstructural changes after CST injury. Its sensitivity may improve when using the peritumoral CST features.

Keywords: *Diffusion magnetic resonance imaging; Glioma; Corticospinal tract; Muscle weakness*

INTRODUCTION

As the most common primary tumor in the brain, glioma accounts for more than 80% of all brain tumors (1-3). It usually grows infiltratively in the white matter and involves the fiber pathway. Accordingly, if the condition affects the corticospinal tract (CST), the most important pathway responsible for intact motor functions, neurosurgeons

Received: June 3, 2020 **Revised:** July 25, 2020 **Accepted:** August 9, 2020
This work was supported by grants from the Natural Science Foundation of Fujian Province (No. 2018J05135), Joint Funds for the innovation of science and Technology, Fujian province (Grant number: 2017Y9024), Training project of young talents in health system of Fujian Province (2018-1-37) and Startup Fund for scientific research, Fujian Medical University (No. 2017XQ1040 and 2019QH1034).
*These authors contributed equally to this work.
Corresponding author: Rifeng Jiang, PhD, Department of Radiology, Fujian Medical University Union Hospital, NO.29 Xinquan Road, Fuzhou 350001, China.
• E-mail: 26630706@qq.com

need to accurately assess CST involvement preoperatively and minimize surgical damage to the CST; its destruction may decrease muscle strength (4). Therefore, it is crucial to provide clinicians with accurate related imaging information.

Over the past decades, diffusion tensor imaging (DTI) has become the preferred method for analyzing diffusion-weighted MR images in anisotropic tissues such as CST (5, 6). DTI can provide surgeons with vital information about eloquent white matter tracts that may be beneficial to the prognosis of patients (7). In addition to the morphological information on CST about the track location, number, length, and volume, DTI also provides several diffusion indices, which may help evaluate CST injuries more reliably (4). However, the underlying assumption of a Gaussian spin displacement distribution in this approach often makes it problematic to interpret the changes in these parameters pathophysiologically. For example, DTI often sensitively predicts functional injuries of the peritumoral white matter in the brain stem, but with a low specificity (8), which may present neurosurgeons with a dilemma and lead to an overestimated destruction of the neural fibers (9). Additionally, fiber-tracking based on DTI sometimes does not accurately estimate the sizes of fiber bundles in pathological conditions, which may lead to post-surgical sequelae such as hemiparesis in the patients (10). Therefore, to assess brain tissue changes comprehensively, it is advisable to resort to an imaging alternative with parameters that are more sensitive and specific than DTI-derived parameters.

A recently proposed diffusion model called mean apparent propagator (MAP) MRI is a mathematical framework connecting the diffusion-weighted imaging q-space with the molecular displacements (11). MAP MRI can accurately reveal microstructure-related features of the white matter, thereby offering better diffusion characteristics in complex tissue structures than DTI. However, in clinical practice the maximum b-value is limited, and noise dominates the signal at higher b-values. To robustly estimate important features from noisy and sparsely sampled data, some researchers proposed to analytically regularize the coefficient estimation of the MAP-MRI method using the norm of the Laplacian of the reconstructed signal. This approach is called the laplacian-regularized MAP (MAPL)-MRI, which can recover important microstructural tissue parameters with less variability, thus contributing to a better understanding of the microstructure-related features of the white matter (12).

MAPL-MRI may have great potential for evaluating brain glioma-induced structural damage to the CST. However, no studies have applied the MAPL-MRI to the prediction of CST damage. Thus, estimating the value of MAPL-MRI in predicting the destruction of the CST is of great clinical significance. Therefore, this study attempted to employ MAPL-MRI to identify the significant CST features that can effectively predict CST injury caused by brain glioma.

MATERIALS AND METHODS

Patients

Patients with suspected gliomas located adjacent to the CST pathway were prospectively enrolled in this study between March 2019 and January 2020, and they underwent preoperative structural and diffusion MRI. This study was approved by the Institutional Review Board of Fujian Medical University Union Hospital (2020KY0132), and written informed consent was obtained from all the participants.

Patients were excluded for the following: poor image quality, namely, obvious artifacts or head motion; surgery performed more than 4 weeks after MR data collection; a large tumor involving the CST on both sides.

Finally, a total of 20 patients (11 males and 9 females; median of age: 53.0 years, with an inter-quartile range of 46.3–62.0 years) with pathologically confirmed glioma were included in this study.

Clinical and Pathological Information

Clinical characteristics, including sex, age, Karnofsky performance status (KPS), and duration of symptoms were recorded. The muscle strengths of the upper and lower limbs were evaluated (grade 0–5) (13). For subjects with inconsistent upper- and lower-limb strengths, the weaker limbs were used for the analysis. Pathologically, the type and grade of the gliomas were determined based on the World Health Organization (WHO) classification criteria (14). The Ki-67 labeling index (LI) and the $IDH1^{R132H}$ mutation status were also recorded.

MRI Data Acquisition

All the images were acquired using a 3T MR scanner (MAGNETOM Prisma, Siemens Healthineers) with a 64-channel receive-only head coil. The structural MR imaging protocols included pre-contrast axial fluid-attenuated inversion recovery (FLAIR) T1-weighted (T1W)

https://doi.org/10.3348/kjr.2020.0949

Korean Journal of Radiology
KJR

images, axial T2-weighted (T2W) fast spin-echo (FSE) images, axial FLAIR T2W images, and subsequent contrast-enhanced axial/sagittal/coronal FLAIR T1W images.

A grid sampling scheme was adopted for acquiring 128 diffusion q-space samples. Different from the shell sampling scheme, the grid sampling scheme sampled the diffusion encoding space using a given grid, which consisted of 14 b-values (250, 500, 750, 1000, 1250, 1500, 2000, 2250, 2500, 2750, 3000, 3250, 3500, and 4000 s/mm^2), along 3, 6, 4, 3, 12, 12, 6, 15, 12, 12, 4, 12, 24, and 3 directions, respectively. The other scan parameters were: repetition time, 3900 ms; echo time, 88 ms; field of view, 230 x 230 mm^2; GeneRalized Autocalibrating Partial Parallel Acquisition, 2; slice acceleration factor, 2; number of averages, 1; voxel size, 2.5 x 2.5 x 2.5 mm^3, without gap; acquisition time, 8 minutes 44 seconds. Because the eddy current artifact produced by the grid sampling scheme cannot be corrected using the eddy current correction, the bipolar pulse was used to regulate the eddy current at the sequence level (15).

Data Postprocessing

Calculation of MAPL-MRI and DTI Parameter Maps

All the diffusion-weighted images were motion-corrected using the Diffusion Kit eddy tool (16). Afterward, the six independent components of the diffusion tensor were estimated, followed by the calculation of fractional anisotropy (FA), mean diffusivity (MD), axial diffusivity (AD), and radial diffusivity (RD). MAPL-MRI parameters were calculated using NeuDiLab, software developed in-house with Python which is based on an open-resource tool called the DIPY Toolbox (https://www.dipy.org/) (17). In brief, the MAP was fit with a radial order of 6. No denoising was applied to the data before MAP fitting, but a positivity constraint and Laplacian regularization with a weighting of 0.05 were applied during fitting (18). Those settings were recommended for robust fitting by the author of the DIPY MAP-MRI toolbox. Finally, MAPL-MRI parameter maps, including mean squared displacement (MSD), q-space inverse variance (QIV), return-to-origin probability (RTOP), return-to-axis probabilities (RTAP) and return-to-plane probabilities (RTPP), were constructed.

CST Tracking and Quantifying

The fiber pathways of the whole brain were reconstructed in DSI-Studio (version Dec 19, 2019 build, http://dsi-studio.labsolver.org/) using generalized q-sampling imaging (GQI) (19) with a diffusion sampling length ratio of 1.25. The restricted diffusion was quantified using restricted diffusion imaging (20). Two experienced radiologists (with 10 and 7 years of experience, respectively) blinded to the patient information tracked the CST that was determined by the selection of fibers passing through seed and target regions of interest (ROIs). The seed ROIs were within the anterior cerebral peduncles (Fig. 1A). The target ROIs were within the primary motor cortex and its underlying white matter area, with the central sulcus served as the posterior border (Fig. 1B). The deterministic streamline tracking algorithm, streamline (Euler), was performed to obtain the entire CST fiber tractography using the default tracking parameters in DSI-Studio (Fig. 1C). The peritumoral CST

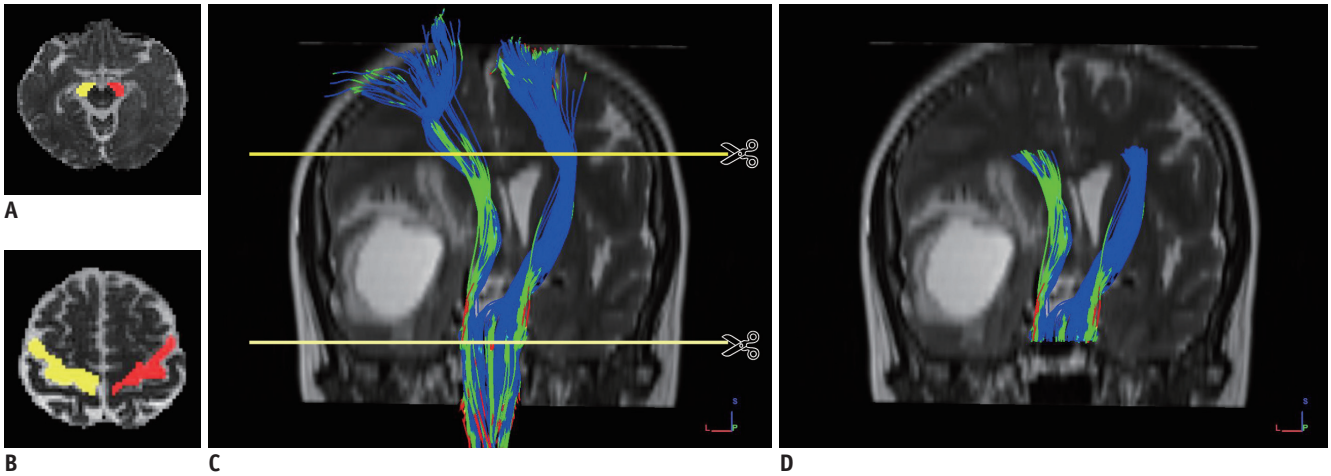

Fig. 1. Reconstruction of the whole and peritumoral CST.
The seed ROIs **(A)** and target ROIs **(B)**. Streamline reconstruction of the CST **(C)**. Segmentation scheme of the peritumoral CST **(D)**. CST = corticospinal tract, L = left, P = posterior, ROI = region of interest, S = superior

https://doi.org/10.3348/kjr.2020.0949

was separated from the whole CST by cutting the superior and inferior segments at the slices where the tumor or its edema disappeared (Fig. 1D). The relationship between the affected CST and the location of the tumor or edema was recorded. Location in the CST pathway meant that the minimum distance between the CST and the tumor or its infiltrating edema was zero, otherwise, the tumor was located near the CST pathway. The entire CST displacement of the affected side was measured based on the location of the healthy CST at the level of the maximum tumor size (Fig. 2) (4). Finally, the number of tracts meant that the tract length (cm) and tract volume (cm^3) of the entire and peritumoral CSTs were evaluated using the "tract statistics" function in DSI-Studio. Subsequently, FA, MD, AD, RD, MSD, QIV, RTOP, RTAP, and RTPP values along the entire and peritumoral CSTs were calculated. The relative FA, MD, AD, RD, MSD, QIV, RTOP, RTAP, and RTPP of the affected CST were calculated as the ratios of the FA, MD, AD, RD, MSD, QIV, RTOP, RTAP, and RTPP of the affected side to those of the healthy side.

Statistical Analysis

Statistical analyses were performed using SPSS software (version 20, IBM Corp.). The paired Wilcoxon test was used to compare the morphological features, including track number, average length and volume, and the diffusion parameter values (AD, RD, FA, MD, MSD, QIV, RTAP, RTOP, and RTPP), of the entire and peritumoral CSTs of the affected side with the corresponding values of the entire and peritumoral CSTs of the healthy side. The Mann-Whitney U test was further performed to compare the difference in the relative CST characteristics (including relative track number, average length, volume, AD, RD, FA, MD, MSD, QIV, RTAP, RTOP, and RTPP) of the entire and peritumoral CSTs between the glioma patients with motor weakness and those with normal motor function. This is an exploratory analysis, and multiple comparisons were not performed.

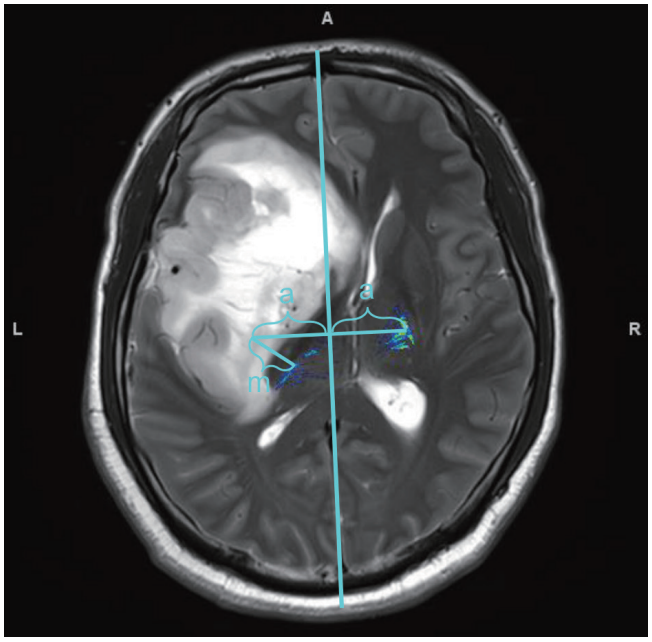

Fig. 2. Measuring displacement of the affected CST.
Displacement of affected CST was determined using the distance (m) between the symmetrical positions of the healthy and actual positions. The vertical distance between the healthy CST and its symmetrical position to the centerline is the same (a). A = anterior

RESULTS

Demographic Characteristics of Participants

The median KPS of the 20 patients was 80 with an inter-quartile range of 70–90. The classification details of the gliomas were as follows: grade II in 11 patients, grade III in 2, and grade IV in 7 according to the WHO classification criteria; 17 were primary and 3 were recurrent gliomas; the median Ki-67 LI was 10.0% with an inter-quartile range of 4.0–37.5%; gliomas in 8 patients were confirmed to carry the $IDH1^{R132H}$ mutation by immunohistochemistry; reduced muscle strength was present in 6 patients, with grade 2 motor weakness in 1 patient, grade 3 in 1, and grade 4 in 4, while the remaining 16 patients showed normal strength; 14 tumors were located in the CST pathway and the remaining were near the CST pathway; the median CST shift was 9.90 mm with an inter-quartile range of 3.62–16.78 mm. The demographic, clinical, and pathological characteristics of the participants are summarized in Table 1.

Changes in CST Features of the Affected Side

Compared with those of the healthy side, the track number, volume, MD, RD, MSD, QIV, RTAP, RTOP, and RTPP of the affected CST changed significantly using the features of the entire CST (p = 0.006, 0.003, 0.004, 0.005, 0.006, 0.002, 0.004, 0.004, and 0.005, respectively) or the features of the peritumoral CST (p = 0.006, 0.015, 0.001, 0.001, 0.001, 0.001, 0.002, 0.001, and 0.001, respectively), whereas the AD and FA changed significantly only for the peritumoral CST (p = 0.002 and 0.021, respectively). The track number and volume, FA, RTAP, RTOP, and RTPP decreased significantly for the affected side, while the AD, MD, RD, MSD, and QIV increased significantly for the affected side. In contrast, no significant difference was

https://doi.org/10.3348/kjr.2020.0949

Korean Journal of Radiology
KJR

Table 1. Demographic, Clinical and Pathological Characteristics of 20 Patients with Glioma

Variable	Values
Age (years)	53.0 [46.3–62.0]
Sex (male)	11 (55.0)
KPS	80 [70–90]
Muscle strength of the limbs	
Grade 5	14 (70.0)
Grade 4	4 (20.0)
Grade 3	1 (5.0)
Grade 2	1 (5.0)
Disease duration (days)	30 [30–135]
In CST pathway	14 (70.0)
CST shift (cm)	9.90 [3.62–16.78]
Recurrent glioma	3 (15.0)
Glioma grade	
Grade II	11 (55.0)
Grade III	2 (10.0)
Grade IV	7 (35.0)
Ki-67 LI(%)	10.0 [4.0–37.5]
$IDH1^{R132H}$ mutation	8 (40.0)

Values are presented as number (%) or median [inter-quartile range]. CST = corticospinal tract, IDH = isocitrate dehydrogenase, KPS = Karnofsky performance status, LI = labeling index

evident between the average lengths of the entire (p = 0.145) and the peritumoral (p = 0.433) CSTs of the two sides. The results are shown in detail in Table 2.

Changes in Relative CST Features in Patients with Motor Weakness

Compared with the glioma patients with normal motor function, the relative MSD (p = 0.039) of the entire CST, QIV of the entire (p = 0.048) and peritumoral (p = 0.021) CSTs as well as the AD (p = 0.026), MD (p = 0.032), and RD (p = 0.048) of the peritumoral CST in patients with motor weakness were significantly higher. The RTPP of the entire (p = 0.021) and peritumoral (p = 0.008) CSTs as well as the RTOP (p = 0.032) of the peritumoral CST in patients with motor weakness were significantly lower. In contrast, no significant changes were observed for the relative CST morphological characteristics, FA and RTAP (p > 0.05 for all). The statistical results are shown in detail in Table 3, and the corresponding box and whisker plot of the relative CST features are shown in Figure 3. Data from two representative patients are shown in Figure 4 to demonstrate the difference between the CST features of the patients with motor weakness and those with normal motor function.

DISCUSSION

MAP-MRI may have great potential in evaluating brain glioma-induced structural damage to the CST; however, an intensive acquisition of MAP-MRI impedes its extensive clinical application (21). In several cases, an accurate estimation of these features takes a long acquisition time due to the large b-values and directions. The original MAP acquisition scheme consists of seven b-values, which are 200, 800, 1800, 3200, 5000, 7200, and 9800 s/mm^2, along 5, 14, 32, 56, 87, 125, and 170 directions, respectively (11). There have been a few attempts to shorten the scan time of q-space imaging, and one can shorten the scan time for the clinical application of MD and zero displacement probability by skipping a few b-values (22). In this study, MAPL-MRI was applied to shorten the scan time and robustly estimate these important features from noisy and sparsely sampled data by analytically regularizing the coefficient estimation of the MAP-MRI method using the norm of the Laplacian of the reconstructed signal. To the best of our knowledge, this is the first application of MAPL-MRI to CST evaluation in brain glioma. The technique was adopted following these considerations (1). MAPL-MRI analysis is usually based on diffusion data using the grid sampling scheme, which acquires data with different b-values and variable sampling density. This scheme has a uniformly distributed density in the diffusion encoding space (q-space). The low b-value range has a lower sampling density, whereas the high b-value range with a higher density makes the entire acquisition much more efficient. The grid sampling scheme captures a continuous range of diffusion patterns from non-restricted diffusion to restricted diffusion. For clinical studies, it can capture all possible diffusion changes due to edematous tissue or cell infiltration. In comparison, multi-shell sampling only acquires 2 or 3 b-values, and it may miss diffusion patterns that are only sensitive to values in between. Therefore, MAPL-MRI may offer a better characterization of diffusion in complex tissue structures like CST, and it can achieve more accurate fiber-bundle tracking in voxels with crossing fibers (2). MAPL-MRI can provide novel quantifiable indices that capture previously obscured intrinsic microstructural features of the nervous tissue, including MSD, QIV, RTOP, RTAP, and RTPP. The RTOP appears to reflect cellularity and restrictions better than MD. The RTAP and RTPP can reflect the restrictive barriers in the radial and axial orientations or heterogeneous diffusion restrictions in the radial and

 https://doi.org/10.3348/kjr.2020.0949

Table 2. Changes in CST Features on the Affected Side

CST Features	Whole CST				Peritumoral CST			
	Affected CST (n = 20)	Healthy CST (n = 20)	Z	*P*	Affected CST (n = 20)	Healthy CST (n = 20)	Z	*P*
Number of tracts	119.50 (79.50–159.75)	198.50 (159.25–228.50)	-2.763	0.006*	119.50 (80.25–159.75)	198.50 (159.25–229.75)	-2.763	0.006*
Average tract length (cm)	14.08 (13.71–14.40)	14.10 (13.81–14.63)	-1.456	0.145	6.99 (4.99–8.95)	7.00 (5.07–9.34)	-0.784	0.433
Tracts volume (cm^3)	25.20 (20.31–28.98)	29.70 (26.72–33.57)	-3.006	0.003*	11.95 (8.36–15.93)	15.38 (10.31–18.55)	-2.427	0.015*
DTI-AD (x 10^{-3} mm^2/s)	0.85 (0.84–0.88)	0.83 (0.815–0.864)	-1.941	0.052	0.88 (0.85–0.92)	0.84 (0.79–0.89)	-3.024	0.002*
DTI-FA	0.53 (0.50–0.55)	0.54 (0.52–0.56)	-1.829	0.067	0.56 (0.49–0.59)	0.57 (0.54–0.62)	-2.315	0.021*
DTI-MD (x 10^{-3} mm^2/s)	0.51 (0.49–0.53)	0.49 (0.48–0.50)	-2.875	0.004*	0.53 (0.49–0.57)	0.48 (0.47–0.49)	-3.397	0.001*
DTI-RD (x 10^{-3} mm^2/s)	0.34 (0.32–0.36)	0.32 (0.31–0.33)	-2.800	0.005*	0.35 (0.30–0.39)	0.29 (0.28–0.33)	-3.211	0.001*
MAPL-MSD (x 10^{-5} mm^2/s)	14.62 (14.23–15.31)	13.97 (13.79–14.32)	-2.725	0.006*	14.59 (13.64–15.47)	13.09 (12.88–13.57)	-3.397	0.001*
MAPL-QIV (x 10^{-10} mm^5/s)	10.86 (9.33–11.95)	9.21 (8.54–9.63)	-3.099	0.002*	11.91 (8.71–14.79)	8.25 (7.87–9.82)	-3.285	0.001*
MAPL-RTAP (x 10^3 mm^{-2}/s)	8.70 (8.06–9.29)	9.31 (8.83–9.74)	-2.875	0.004*	8.66 (7.98–10.04)	10.19 (9.49–10.71)	-3.099	0.002*
MAPL-RTOP (x 10^3 mm^{-2}/s)	5.79 (5.32–6.14)	6.31 (6.01–6.58)	-2.912	0.004*	5.86 (4.98–6.63)	6.90 (6.51–7.27)	-3.285	0.001*
MAPL-RTPP (x 10^3 mm^{-2}/s)	5.27 (5.17–5.32)	5.33 (5.26–5.40)	-2.800	0.005*	5.21 (5.11–5.28)	5.37 (5.24–5.59)	-3.435	0.001*

Dara are presented as median (inter-quartile range). *Represented a statistical difference ($p < 0.05$). AD = axial diffusivity, DTI = diffusion tensor imaging, FA = fractional anisotropy, MAPL = laplacian-regularized mean apparent propagator, MD = mean diffusivity, MSD = mean squared displacement, QIV = q-space inverse variance, RD = radial diffusivity, RTAP = return-to-axis probabilities, RTOP = return-to-origin probability, RTPP = return-to-plane probabilities

axial directions. These scalar parameters encode directional information well-suited for characterizing complex diffusion in anisotropic tissues, and they can potentially distinguish whiter matter biomarkers for axonal loss or demyelination (11).

In this study, the results showed that the track number, volume, MD, RD, MSD, QIV, RTAP, RTOP, and RTPP of the entire CST changed significantly for the affected CST. When using the peritumoral CST features, all the features, except the average track length, changed significantly for the affected side. All the parameters of MAPL-MRI for the CST of the affected side were significantly different from those of the healthy side. In contrast, only MD and RD of the DTI changed significantly, which indicates that MAPL-MRI parameters are more sensitive than some of the DTI parameters, such as FA, in evaluating abnormalities of CST. In addition, the peritumoral CST features seem to be more sensitive in revealing the CST abnormality of the affected side. No significant change was found between the average track lengths of the CSTs of the affected and the healthy sides, which may have been due to the incomplete destruction or interruption of the CSTs.

Previous studies have shown that damage to the CST can result in motor weakness (4, 19). The latter can serve as an indicator of CST damage in patients with glioma. Therefore, this study further investigated the relationship between CST features and motor function to find the effective features that were indicative of CST damage. CST features, such as FA, vary across individuals and different ages although they have good bilateral symmetry (23); therefore, we used the relative CST features to minimize the effects of age and individual variation. We found that the relative MSD and QIV along the entire CST increased, but RTPP decreased significantly in patients with motor weakness. When the

https://doi.org/10.3348/kjr.2020.0949

Korean Journal of Radiology
KJR

Table 3. Changes in Relative CST Features in Patients with Motor Weakness

Relative CST Features	Whole CST				Peritumoral CST			
	Normal Motor Function (n = 14)	Motor Weakness (n = 6)	Z	*P*	Normal Motor Function (n = 14)	Motor Weakness (n = 6)	Z	*P*
Displacement of affected CST (cm)	7.36 (3.59–14.30)	15.15 (3.80–19.04)	-0.949	0.343	-	-	-	-
Number of tracts	0.61 (0.41–0.86)	0.55 (0.38–1.40)	-0.330	0.741	0.60 (0.42–0.86)	0.55 (0.38–1.40)	-0.330	0.741
Average tract length	0.98 (0.97–1.00)	1.02 (0.94–1.06)	-1.155	0.248	0.98 (0.97–1.02)	1.04 (0.96–1.06)	-0.907	0.364
Tracts volume	0.85 (0.76–0.92)	0.81 (0.62–1.08)	-0.165	0.869	0.84 (0.75–0.93)	0.83 (0.55–1.12)	0.000	1.000
DTI-AD	1.00 (0.99–1.03)	1.07 (1.00–1.11)	-1.897	0.058	1.05 (1.01–1.08)	1.13 (1.09–1.22)	-2.227	0.026*
DTI-FA	0.97 (0.93–1.02)	0.95 (0.94–1.01)	-0.825	0.409	0.95 (0.91–1.05)	0.94 (0.93–0.95)	-0.660	0.509
DTI-MD	1.02 (1.00–1.05)	1.11 (1.03–1.13)	-1.815	0.070	1.04 (1.00–1.13)	1.22 (1.08–1.34)	-2.144	0.032*
DTI-RD	1.05 (0.99–1.09)	1.15 (1.07–1.17)	-1.732	0.083	1.11 (0.98–1.22)	1.28 (1.08–1.40)	-1.979	0.048*
MAPL-MSD	1.02 (1.00–1.06)	1.11 (1.01–1.12)	-2.062	0.039*	1.04 (1.00–1.14)	1.22 (1.08–1.32)	-1.897	0.058
MAPL-QIV	1.07 (1.02–1.20)	1.38 (1.16–1.42)	-1.979	0.048*	1.15 (0.98–1.49)	1.71 (1.20–2.16)	-2.309	0.021*
MAPL-RTAP	0.96 (0.91–1.01)	0.88 (0.82–0.94)	-1.897	0.058	0.92 (0.83–1.02)	0.75 (0.73–0.94)	-1.815	0.070
MAPL-RTOP	0.96 (0.91–1.01)	0.84 (0.79–0.94)	-1.897	0.058	0.93 (0.81–1.00)	0.70 (0.65–0.90)	-2.144	0.032*
MAPL-RTPP	0.99 (0.98–1.00)	0.96 (0.95–0.99)	-2.309	0.021*	0.97 (0.96–0.99)	0.94 (0.89–0.95)	-2.639	0.008*

Dara are presented as median (inter-quartile range). "-" represented not applicable. *Represented a statistical difference ($p < 0.05$).

peritumoral CST features were used, more relative diffusion parameters (QIV, AD, MD, RD, RTPP, and RTOP) became significant, and QIV, AD, MD, and RD increased, but RTPP and RTOP decreased significantly in patients with motor weakness. These findings suggest that the relative MAPL-MRI features may be more sensitive indicators of CST injury, and the sensitivity can be further improved by using the peritumoral CST features.

The changes in the relative diffusion parameters in patients with motor weakness can be explained by the destruction of the diffusion barriers in the affected CST. Long-term infiltration of the glioma may lead to a change in the integrity of the CST, including a decrease in the number of neural fibers and demyelination, thereby leading to a decrease in the diffusion barrier. The decrease in the number of neural fibers and demyelination influences the conduction of the nerve fiber in the CST, which may cause motor weakness. Of the MAPL-MRI parameters, the RTOP reflects the cellularity or diffusion restrictions in the microstructure, and the RTAP and RTPP reflect the restrictive barriers in the radial and axial orientations. Therefore, the relative RTOP and RTPP decreased significantly, and RTAP also decreased, although it did not reach a significant level. The increased MSD value of the affected side reflects enhanced free diffusion of water molecules, due to the loss of anisotropy of water molecules that is caused by the impaired fiber integrity. QIV was higher for the CST of the affected side. Similarly, a previous study reported that QIV suggested abnormalities in multiple sclerosis with the highest statistical significance among all metrics (24, 25). The relative AD, MD, and RD also increased due to the destruction of the diffusion barriers in the affected CST, which increases the diffusivity. However, no significant difference in relative FA was found, which was different

 https://doi.org/10.3348/kjr.2020.0949

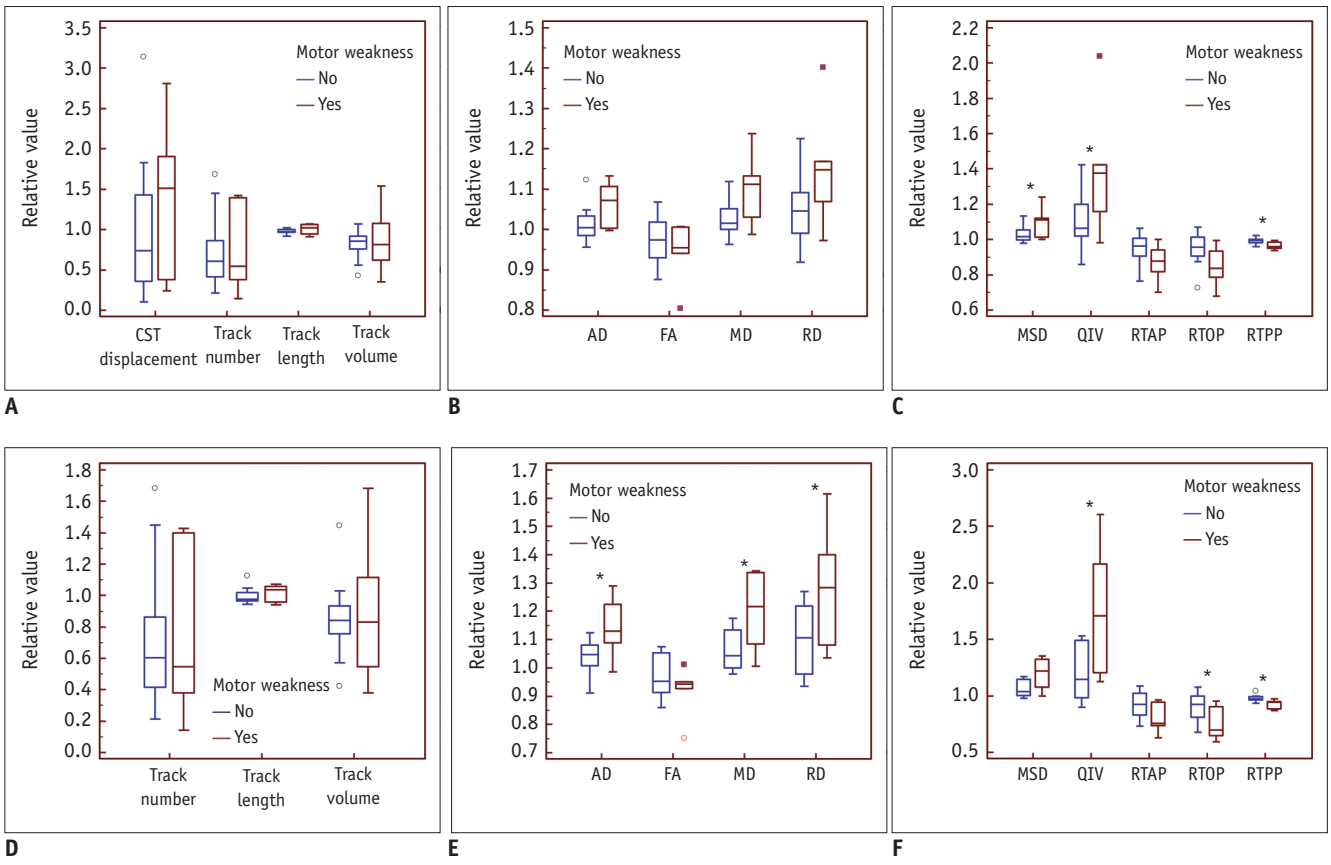

Fig. 3. Changes in the relative CST features in patients with motor weakness.
Box and whisker plot of the relative CST features of the entire **(A-C)** and the peritumoral **(D-F)** CSTs showed that the relative MSD of the entire CST and QIV of the entire and peritumoral CSTs as well as the AD, MD, and RD of the peritumoral CST in patients with motor weakness were significantly higher (*). The RTPP of the entire and peritumoral CSTs and the RTOP of the peritumoral CST in patients with motor weakness were significantly lower (*). In contrast, no significant changes were found between the relative CST morphological characteristics, FA, and RTAP.
AD = axial diffusivity, FA = fractional anisotropy, MD = mean diffusivity, QIV = q-space inverse variance, RD = radial diffusivity, RTAP = return-to-axis probabilities, RTOP = return-to-origin probability

from the results in the previous studies (4, 26, 27). The discrepancy suggests that FA may be an unstable or controversial parameter. Previous studies have demonstrated that MAP-MRI parameters can better reflect microstructural changes in white and grey matter (28). A recent study shows that RTOP tissue contrast may better reflect overall restrictions and cellularity than MD (5). RTOP can be decomposed in the local anatomical frame of reference determined by the orientation of the diffusion tensor, and it reveals additional information complementary to DTI. Similarly, the relative MAPL-MRI features in this study were also more sensitive indicators of CST damage. The sensitivity was further improved by using the peritumoral CST features; the change may have been more obvious in the peritumoral CST.

In contrast, the present study found the relative morphological features, including track number, volume, average length, and displacement of CST, showed no significant difference between patients with motor weakness and those with normal motor function. Previous studies suggested that evaluating neural fiber injury using quantificational DTI metrics was more reliable than evaluating morphological changes (4). Therefore, the conclusion in the current study is consistent with that of the previous study.

Unlike previous studies researching the CST adjacent to different kinds of brain tumors (4), this study focused only on the effect of gliomas on CST. Glioma is different from other intracranial tumors such as metastasis and meningioma. Inclusion of only glioma patients would eliminate the influence of the tumor category on the final results. In addition, the previous studies focused mainly on the entire CST, but the tumors usually only involve the peritumoral CST, so the measurement of the entire CST may

https://doi.org/10.3348/kjr.2020.0949

Korean Journal of Radiology
KJR

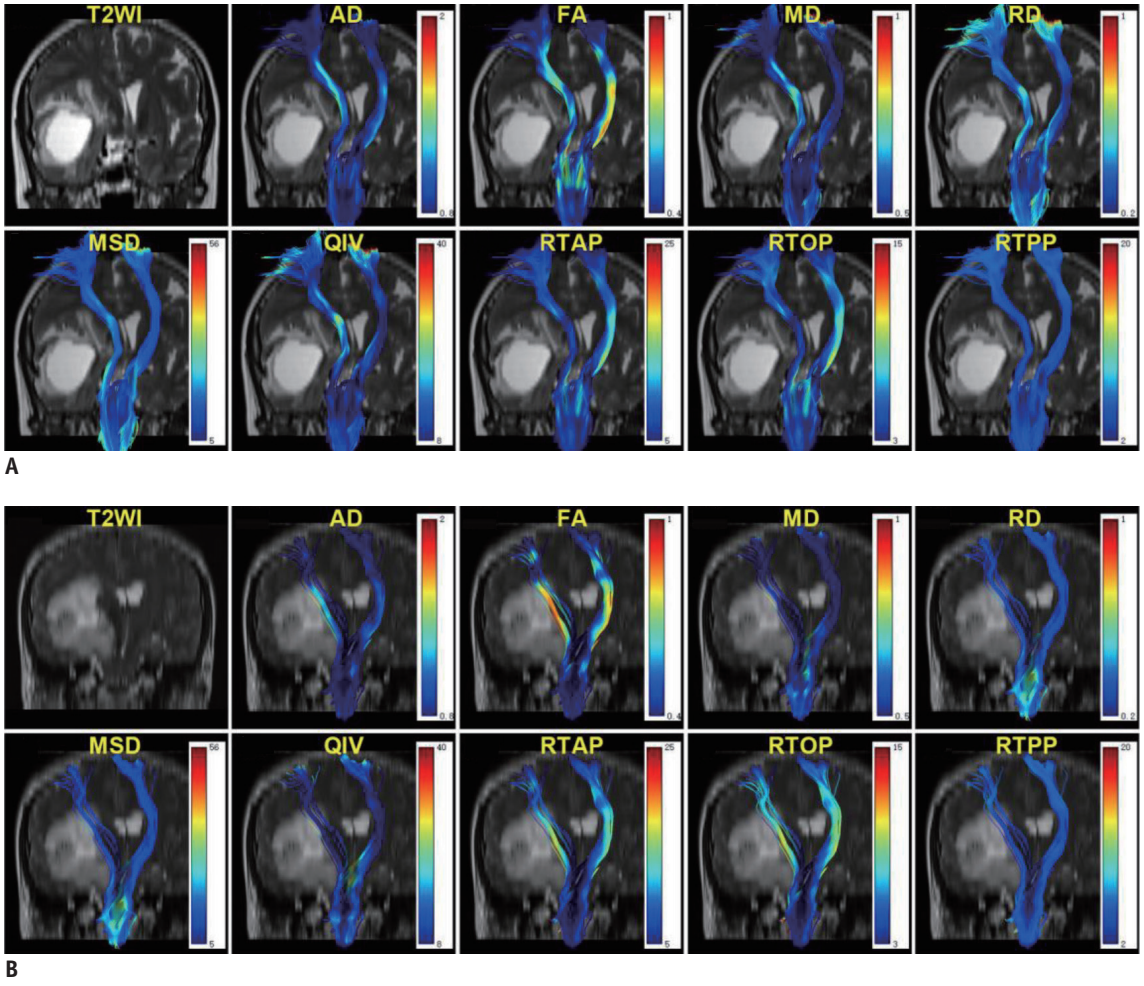

Fig. 4. Two representative patients demonstrating the CST changes of glioma-induced injury.
Coronal T2WI, DTI, and MAPL maps for two representative patients demonstrating the difference between the CST features in patients with motor weakness and those with normal motor function. The first patient **(A)** was a 62-year-old female with glioblastoma (WHO grade IV), and she had motor weakness (grade 2). Changes in the affected CST were obvious in almost all the diffusion maps except the RTPP, but not in track number or volume. The second patient **(B)** was a 39-year-old male with oligodendroglioma (WHO grade II), and his motor function was normal. Changes in the affected CST were obvious in the track number or volume, but not in all the diffusion maps except the AD. T2WI = T2-weighted image, WHO = World Health Organization

decrease the sensitivity of indicators for CST damage. In the current study, the features of the entire and peritumoral CSTs were used to evaluate motor weakness. It was found that the sensitivity of CST damage evaluation increased when the features of the peritumoral CST were considered.

There are some limitations to this study. First, there was no direct correlation between diffusion-sampled data and surgical findings; therefore, it could not be ascertained whether the glioma truly infiltrated the CST. However, the decrease in the muscle strength of the limbs may indirectly reflect the injury of CST (4). Second, the fiber tracking method may not have displayed complete CST bundles, even though a GQI algorithm based on q-space data was used to maximize the reduction in cross-fibers in the CST bundles (29, 30). Additionally, the results of our analysis were mainly limited by the relatively small patient cohort. Therefore, this study did not use the receiver operating characteristic curve to further compare the diagnostic efficiency of MAPL-MRI with that of DTI. However, we believe the conclusions are still valuable for clinical practice.

In conclusion, MAPL-MRI may be a more effective approach for evaluating the CST injury. Its sensitivity may improve when the peritumoral CST features are considered. Therefore, MAPL-MRI may serve as a method for demonstrating the microstructural changes in the affected CST, which may achieve a more accurate diagnosis and optimal therapy for glioma patients.

https://doi.org/10.3348/kjr.2020.0949

Conflicts of Interest

The authors have no potential conflicts of interest to disclose.

ORCID iDs

Rifeng Jiang
https://orcid.org/0000-0001-6959-0027
Zhongshuai Zhang
https://orcid.org/0000-0002-1594-0906

REFERENCES

1. Lapointe S, Perry A, Butowski NA. Primary brain tumours in adults. *Lancet* 2018;392:432-446
2. Goodenberger ML, Jenkins RB. Genetics of adult glioma. *Cancer Genet* 2012;205:613-621
3. Ostrom QT, Bauchet L, Davis FG, Deltour I, Fisher JL, Langer CE, et al. The epidemiology of glioma in adults: a "state of the science" review. *Neuro Oncol* 2014;16:896-913
4. Min ZG, Niu C, Zhang QL, Zhang M, Qian YC. Optimal factors of diffusion tensor imaging predicting corticospinal tract injury in patients with brain tumors. *Korean J Radiol* 2017;18:844-851
5. Avram AV, Sarlls JE, Barnett AS, Özarslan E, Thomas C, Irfanoglu MO, et al. Clinical feasibility of using mean apparent propagator (MAP) MRI to characterize brain tissue microstructure. *Neuroimage* 2016;127:422-434
6. Basser PJ, Mattiello J, LeBihan D. Estimation of the effective self-diffusion tensor from the NMR spin echo. *J Magn Reson B* 1994;103:247-254
7. Zakaria H, Haider S, Lee I. Automated whole brain tractography affects preoperative surgical decision making. *Cureus* 2017;9:e1656
8. Kovanlikaya I, Firat Z, Kovanlikaya A, Uluğ AM, Cihangiroglu MM, John M, et al. Assessment of the corticospinal tract alterations before and after resection of brainstem lesions using diffusion tensor imaging (DTI) and tractography at 3T. *Eur J Radiol* 2011;77:383-391
9. Min ZG, Rana N, Niu C, Ji HM, Zhang M. Does diffusion tensor tractography of the corticospinal tract correctly reflect motor function? *Med Princ Pract* 2014;23:174-176
10. Kinoshita M, Yamada K, Hashimoto N, Kato A, Izumoto S, Baba T, et al. Fiber-tracking does not accurately estimate size of fiber bundle in pathological condition: initial neurosurgical experience using neuronavigation and subcortical white matter stimulation. *Neuroimage* 2005;25:424-429
11. Özarslan E, Koay CG, Shepherd TM, Komlosh ME, İrfanoğlu, MO, Pierpaoli C, et al. Mean apparent propagator (MAP) MRI: a novel diffusion imaging method for mapping tissue microstructure. *Neuroimage* 2013;78:16-32
12. Fick RHJ, Wassermann D, Caruyer E, Deriche R. MAPL: tissue microstructure estimation using Laplacian-regularized MAP-MRI and its application to HCP data. *Neuroimage* 2016;134:365-385
13. Cuthbert SC, Goodheart GJ Jr. On the reliability and validity of manual muscle testing: a literature review. *Chiropr Osteopat* 2007;15:4
14. Louis DN, Perry A, Reifenberger G, von Deimling A, Figarella-Branger D, Cavenee WK, et al. The 2016 World Health Organization classification of tumors of the central nervous system: a summary. *Acta Neuropathol* 2016;131:803-820
15. Miao HC, Wu MT, Kao EF, Chiu YH, Chou MC. Comparisons of reproducibility and mean values of diffusion tensor imaging-derived indices between unipolar and bipolar diffusion pulse sequences. *J Neuroimaging* 2015;25:892-899
16. Xie S, Chen L, Zuo N, Jiang T. DiffusionKit: a light one-stop solution for diffusion MRI data analysis. *J Neurosci Methods* 2016;273:107-119
17. Garyfallidis E, Brett M, Amirbekian B, Rokem A, van der Walt S, Descoteaux M, et al. Dipy, a library for the analysis of diffusion MRI data. *Front Neuroinform* 2014;8:8
18. Fick RHJ, Wassermann D, Sanguinetti G, Deriche R. *Laplacian-regularized MAP-MRI: Improving axonal caliber estimation*. Proceedings of 2015 IEEE 12th International Symposium on Biomedical Imaging (ISBI); April 16-19, 2015; 2015: New York, NY, USA.
19. Melhem ER, Mori S, Mukundan G, Kraut MA, Pomper MG, van Zijl PC. Diffusion tensor MR imaging of the brain and white matter tractography. *AJR Am J Roentgenol* 2002;178:3-16
20. Yeh FC, Liu L, Hitchens TK, Wu YL. Mapping immune cell infiltration using restricted diffusion MRI. *Magn Reson Med* 2017;77:603-612
21. Olson DV, Arpinar VE, Muftuler LT. Optimization of q-space sampling for mean apparent propagator MRI metrics using a genetic algorithm. *Neuroimage* 2019;199:237-244
22. Sakai K, Yamada K, Akazawa K, Tazoe J, Yasuike M, Nagano H, et al. Can we shorten the q-space imaging to make it clinically feasible? *Jpn J Radiol* 2017;35:16-24
23. Reich DS, Smith SA, Jones CK, Zackowski KM, van Zijl PC, Calabresi PA, et al. Quantitative Characterization of the Corticospinal Tract at 3T. *AJNR Am J Neuroradiol* 2006;27:2168-2178
24. Assaf Y, Blumenfeld-Katzir T, Yovel Y, Basser PJ. AxCaliber: a method for measuring axon diameter distribution from diffusion MRI. *Magn Reson Med* 2008;59:1347-1354
25. Ma K, Zhang X, Zhang H, Yan X, Gao A, Song C, et al. Mean apparent propagator-MRI: a new diffusion model which improves temporal lobe epilepsy lateralization. *Eur J Radiol* 2020;126:108914
26. Wang M, Ma H, Wang X, Guo Y, Xia X, Xia H, et al. Integration of BOLD-fMRI and DTI into radiation treatment planning for high-grade gliomas located near the primary motor cortexes and corticospinal tracts. *Radiat Oncol* 2015;10:64
27. Panara V, Navarra R, Mattei PA, Piccirilli E, Bartoletti V, Uncini A, et al. Correlations between cervical spinal cord magnetic resonance diffusion tensor and diffusion kurtosis

imaging metrics and motor performance in patients with chronic ischemic brain lesions of the corticospinal tract. *Neuroradiology* 2019;61:175-182
28. Cavarsan CF, Malheiros J, Hamani C, Najm I, Covolan L. Is mossy fiber sprouting a potential therapeutic target for epilepsy? *Front Neurol* 2018;9:1023
29. Yeh FC, Wedeen VJ, Tseng WY. Generalized q-sampling imaging. *IEEE Trans Med Imaging* 2010;29:1626-1635
30. Jin Z, Bao Y, Wang Y, Li Z, Zheng X, Long S, et al. Differences between generalized Q-sampling imaging and diffusion tensor imaging in visualization of crossing neural fibers in the brain. *Surg Radiol Anat* 2019;41:1019-1028

https://doi.org/10.3348/kjr.2020.0949